Intermediate Conductances during Deactivation of Heteromultimeric *Shaker* Potassium Channels

Jie Zheng and Fred J. Sigworth

From the Department of Cellular and Molecular Physiology, Yale University School of Medicine, New Haven, Connecticut 06520

ABSTRACT A previous study of the T442S mutant *Shaker* channel revealed activation-coupled subconductance levels that apparently represent kinetic intermediates in channel activation (Zheng, J., and F.J. Sigworth. 1997. *J. Gen. Physiol.* 110:101–117). We have now extended the study to heteromultimeric channels consisting of various numbers of mutant subunits as well as channels without mutant subunits, all in the background of a chimeric *Shaker* channel having increased conductance. It has been found that activation-coupled sublevels exist in all these channel types, and are traversed in at least 80% of all deactivation time courses. In symmetric K^+ solutions, the currents in the two sublevels have a linear voltage dependence, being 23–44% and 54–70% of the fully open conductance. Sublevels in different channel types share similar voltage dependence of the mean lifetime and similar ion selectivity properties. However, the mean lifetime of each current level depends approximately geometrically on the number of mutant subunits in the channel, becoming shorter in channels having fewer mutant subunits. Each mutant subunit appears to stabilize all of the conducting states by ~0.5 kcal/mol. Consistent with previous results in the mutant channel, sublevels in channels with two or no mutant subunits also showed ion selectivities that differ from that of the fully open level, having relatively higher K^+ than Rb^+ conductances. A model is presented in which *Shaker* channels have two coupled activation gates, one associated with the selectivity filter and a second associated with the S6 helix bundle.

KEY WORDS: ion channel gating • selectivity • subconductance • cooperativity • subunit stoichiometry

INTRODUCTION

The activation of *Shaker* potassium channels involves many conformational changes. A study by Cole and Moore (1960) showed that 25 independent transitions would be required to explain the activation delay in squid axon potassium currents. Analysis of the time course of *Shaker* channel opening in response to a voltage step shows that, as a minimum, five to seven sequential transitions must occur during channel activation (Zagotta et al., 1994*a*; Schoppa and Sigworth, 1998*a*). Gating current measurements from *Shaker* potassium channels (Stühmer et al., 1991; Schoppa et al., 1992; Perozo et al., 1993) and voltage-gated sodium channels (Conti et al., 1984; Vandenberg and Bezanilla, 1991) suggest that the voltage-dependent conformational changes comprise multiple steps and are not identical. The *Shaker* channel is composed of four identical α subunits (MacKinnon, 1991; Kavanaugh et al., 1992; Li et al., 1994). Some cooperativity between subunits during the activation process seems likely. Evidence for cooperativity in gating and block has been obtained in *Shaker* wild-type and mutant channels (Tytgat and Hess, 1992; Liman et al., 1992; Heginbotham and MacKinnon, 1992; Schoppa et al., 1992; Ogielska et al., 1995) and is required to model *Shaker* channel activation gating (Zagotta et al., 1994*b*; Bezanilla et al., 1994; Schoppa and Sigworth, 1998*b*).

Attempts have been made to isolate different steps in the *Shaker* channel activation time course by manipulating the testing protocols for macroscopic and gating currents (Zagotta et al., 1994*a*; Bezanilla et al., 1994; Schoppa and Sigworth, 1998*a*). In most cases, however, it has been difficult to isolate any of the intermediate steps. Chapman et al. (1997) found activation-dependent subconductance levels in single-channel recordings of the Kv2.1 channel. They concluded that these sublevels represent partially activated channel states in which the pore-forming regions of the various subunits have nonequivalent conformations. Our previous study of the *Shaker* channel pore mutant T442S has identified two sublevels that are predominantly seen during channel activation and deactivation (Zheng and Sigworth, 1997). The occurrence of these sublevels is kinetically distinct from the subconductance behavior that is occasionally seen in wild-type *Shaker* channels (Hoshi et al., 1994; Schoppa and Sigworth, 1998*a*), whose occurrence appears to be unrelated to the activation process. In T442S channels, the larger sublevel is always traversed during channel activation and deactivation. Transitions between the two sublevels and between the larger sublevel and the open level involve identical

Address correspondence to F.J. Sigworth, Department of Cellular and Molecular Physiology, Yale University School of Medicine, 333 Cedar Street, New Haven, CT 06520. Fax: 203-785-4951; E-mail: fred.sigworth @yale.edu

charge movements, consistent with the idea that each of these transitions arise from equivalent motions occurring in separate subunits. The fact that sublevels of the T442S mutant channel have differing ion selectivities provides a hint that some of the pore structure may be involved in the conformational changes that lead to the channel opening.

The present paper is the second on a series of studies of *Shaker* channel sublevels. We made use of the tetrameric nature of *Shaker* channels to study the effect of each subunit on the sublevel behavior. Heteromultimeric channels incorporating various numbers of T442S mutant subunits were obtained by coexpression of the T442S cRNA and its parental cRNA (actually a *Shaker*-mKv3.1 chimera, which we nevertheless shall refer to as WT).[1] Heteromultimeric channels were also studied by expressing tandem dimer constructs containing cDNAs encoding the two types of subunits. We also included in this study the WT homomultimeric channels. The experiments were designed to answer two questions: first, do sublevels exist in the heteromultimeric and WT channels, and second, if sublevels exist, what is the relationship between sublevels and the final steps in channel activation?

METHODS

cDNA Constructs and Oocyte Expression

The two subunit types used in this study have been previously described (Zheng and Sigworth, 1997). The "wild-type" subunit (W) is a *Shaker B* chimera (Lopez et al., 1994) in which the S6 segment is substituted by the S6 sequence of the mKv3.1 (also known as NGK2) potassium channel; the NH_2-terminal inactivation sequence is also removed. The tetrameric WT channel (W_4) has a single-channel conductance approximately fourfold larger than *Shaker* when expressed in *Xenopus* oocytes; the gating kinetics seem to be unchanged. The "mutant" subunit (M) carries a pore mutation T442S in the WT background. Both cDNAs were carried by the pBluescript vector (Stratagene Inc., La Jolla, CA).

Heteromultimeric channels were made by coexpressing WT and mutant subunit cRNAs in *Xenopus* oocytes, and the stoichiometry identified by the conductance and kinetics of the single-channel currents (see RESULTS). Heteromultimeric channels were also made by tandem dimer constructs in which two cDNAs were linked together with a sequence encoding a linker peptide 24–64 amino acids in length (J. Zheng, Y. Yan, and F.J. Sigworth, manuscript in preparation). The linker sequence replaces the stop codon of the first protomer. Each construct was verified by restriction mapping. All dimers were carried by the pGEM-A vector (Swanson et al., 1990).

The monomer cDNAs were linearized with EcoO109I and cRNAs were transcribed with the MEGAscript T_3 RNA polymerase kit (Ambion Inc., Austin, TX). The dimer cDNAs were linearized with NotI and cRNAs were transcribed with the MEGAscript T_7 RNA polymerase kit. Sizes of the transcribed cRNAs were verified by gel electrophoresis.

[1]*Abbreviations used in this paper:* M, mutant subunit; W or WT, *Shaker*-mKv3.1 chimera.

Oocyte preparation and injection protocols were identical to those previously described (Zheng and Sigworth, 1997), except that ND96 solution replaced the OR3 solution in which defolliculated stage V-VI oocytes were stored at 20°C. ND96 contained 96 mM NaCl, 2 mM KCl, 1.8 mM $CaCl_2$, 1 mM $MgCl_2$, 50 U/ml penicillin, 50 ng/ml streptomycin, and 5 mM HEPES, adjusted to pH 7.4 with NaOH. 50 nl of cRNA was injected into *Xenopus* oocytes using a microinjector (Drummond Scientific Co., Broomall, PA). Concentrations of injected cRNAs were measured with a spectrophotometer (Spectronic 1001; Bausch and Lomb, Rochester, NY) and were varied by dilution to control the level of expression.

Single Channel Recording

Single-channel recordings were made from inside-out patches, and in some cases from cell-attached patches. No obvious difference was observed in the kinetics and conductance between data recorded by the two recording methods. Patch pipettes were pulled from 7052 glass (Garner Glass, Claremont, CA) with 1–2.5-μm tip diameters, and were coated with Sylgard (Dow Corning Co., Midland, MI). The pipette solution contained 140 mM K-Aspartate, 1.8 mM $CaCl_2$, 10 mM HEPES, and the bath solution contained 130 mM K-Aspartate, 10 mM KCl, 1 mM EGTA, 10 mM HEPES, adjusted to pH 7.3 with KOH. The liquid junction potential at the interface of these two solutions was estimated to be 0.8 mV; no correction was applied. For selectivity experiments, Rb^+ substituted K^+ in the pipette solution.

Most of the experiments were carried out using an EPC-9 patch clamp amplifier and the Pulse software (HEKA-Electronic, Lambrecht, Germany). Voltage pulses were applied from a holding potential of −100 mV. Current signals were filtered at 2.5 kHz, and data were sampled at 12.5 kHz. Recordings from the W_4 channels were made using an Axopatch 200B amplifier (Axon Instruments, Foster City, CA); the signal was filtered at 10 kHz and sampled at 40 kHz. Leak subtraction was performed using an average of the nearest null traces.

Data Analysis

Analysis of the single channel recordings was made using various user-developed programs in the PowerMod environment (HEKA-Electronic) using the Modula-2 language. A digital Gaussian filter was used to further filter the data as required to achieve an appropriate signal-to-noise ratio. Event detection was performed using the threshold-crossing analysis method (Colquhoun and Sigworth, 1995). We used a set of three thresholds to detect transitions among multiple current levels, or two thresholds to determine the total transition time. Amplitude histograms were used for kinetic analysis. A mixture of Gaussian functions was fitted by least squares to the histograms using the Igor data analysis program (WaveMetrics, Lake Oswego, OR).

Statistical quantities are given as mean ± SD.

Binomial Fitting

The distribution of channel types recorded from oocytes coinjected with WT and mutant cRNAs was fitted with a binomial distribution. This was done by the maximum likelihood method, which estimates as P, the probability of incorporating a mutant subunit:

$$P = \frac{\sum_{n=0}^{4} n q_n}{4 \sum_{n=0}^{4} q_n}, \qquad (1)$$

in which q_n is the number of observed channels having n mutant subunits, $n = 0$–4.

Distribution of Transition Times

The transition time of single-channel closure was measured as the time between crossing thresholds 90 and 10% of the fully open current level. Maximum-likelihood fitting was applied to individual measurements according to the following theory. Given an instantaneous current transition of unit amplitude at time zero, the time t_i of crossing threshold θ_i is determined by both the filter characteristics (Colquhoun and Sigworth, 1995) and the current noise n_i at that time, such that the following equation holds for the filter step response $H(t)$:

$$H(t_i) = \theta_i - n_i . \quad (2)$$

The time spent between the crossings of the two thresholds θ_1 and θ_2 is then given by

$$s = H^{-1}(\theta_2 - n_2) - H^{-1}(\theta_1 - n_1) , \quad (3)$$

where $H^{-1}(y)$ is the inverse function of $H(t)$. In turn, s can be approximated to first order in n_1 and n_2 by

$$s \approx [H^{-1}(\theta_2) - H^{-1}(\theta_1)] + [k_1 n_1 - k_2 n_2] , \quad (4)$$

where

$$k_i = \left. \frac{dH^{-1}(y)}{dy} \right|_{y = \theta_i} .$$

Assuming n_1 and n_2 to be independent Gaussian random variables, Eq. 4 suggests that s can be approximated as a Gaussian random variable with mean $\mu_s = H^{-1}(\theta_2) - H^{-1}(\theta_1)$ and variance $\sigma_s^2 = (k_1\sigma_1)^2 + (k_2\sigma_2)^2$. Thus, the probability density of s can be written:

$$f_0(s) = \frac{1}{\sqrt{2\pi}\sigma_s} \exp[-(s-\mu_s)^2/2\sigma_s^2] . \quad (5)$$

When a closure traverses one or two sublevels whose lifetimes are exponentially distributed with means τ_1 and τ_2, the total transition time has a probability density function that is a weighted sum of the two exponential functions convolved with f_0,

$$f_1(s) = \int_0^s f_0(s-t) \left[\frac{A_1}{\tau_1} \exp(-t/\tau_1) + \frac{A_2}{\tau_2} \exp(-t/\tau_2) \right] dt . \quad (6)$$

When only one sublevel is traversed, the amplitude A_2 is zero. On the other hand, if both sublevels are always traversed, the amplitudes are constrained by the relation

$$\frac{A_1}{\tau_1} + \frac{A_2}{\tau_2} = 0 ,$$

with $A_1 > 0$ in the case that $\tau_1 > \tau_2$.

RESULTS

Identification of Channel Stoichiometries

Currents in the homomeric WT and mutant channels differ in three aspects (Zheng and Sigworth, 1997; see Fig. 1, *top* and *bottom*). First, the W_4 channel deactivates quickly; at −100 mV the tail current decays to its half-maximum amplitude in 1.5 ms. The M_4 channel has tail currents that decay two to three orders of magnitude more slowly; at −100 mV the half-decay time is ~600 ms. Second, consistent with the fast deactivation shown in the macroscopic currents, the single channel currents recorded from the W_4 channel have a short mean open time and many brief closures. The M_4 channel has stable openings and a remarkably long mean open time even at very hyperpolarized potentials. Finally, the two channel types differ in their single-channel conductance. The W_4 channel has a mean conductance of 94.7 ± 0.8 pS (n = 12). The M_4 channel has a mean conductance of 28.3 ± 0.9 pS (n = 19), more than three times smaller than the W_4 channel.

We injected various mixtures of WT and mutant cRNAs into *Xenopus* oocytes. As the *Shaker* channels are tetramers, if the WT and mutant subunits assemble randomly to form a channel, one should expect three or four heteromultimeric channel types with various stoichiometries. When a large number of single channel recordings was made, we indeed found four populations of single channels besides the two homomultimeric channels (Fig. 1 *A*). These channel types have single channel conductances of 52.9 ± 4.7 pS (n = 23), 72.3 ± 1.0 pS (n = 18), 78.6 ± 0.9 pS (n = 15), and 88.8 ± 0.9 pS (n = 19). Interestingly, the gating kinetics of these channel populations also showed intermediate phenotypes in such a way that the channels with higher conductance had shorter mean open time and more brief closures (similar to the W_4 channel), and the channels with lower conductance had longer mean open times and were more stable (similar to the M_4 channel). We take the parallel changes in conductance and kinetic properties to reflect various numbers of mutant subunits in the channel tetramer. Accordingly, in Fig. 1 *D* we give a tentative assignment of subunit stoichiometries to each channel population.

Assuming that the WT and mutant subunits assemble randomly into tetramers, our assignment of stoichiometries can be tested by the way in which the frequencies of channel populations vary as the ratio of WT to mutant cRNA is varied. We coinjected WT and mutant cRNAs at four different ratios (1:1, 1:1.3, 1:2, and 1:4). As shown in Fig. 2, coinjection at the 1:1 ratio yielded channels mainly of the higher conductances. This is expected if the mutant cRNA has reduced competence for translation into functional subunits, as suggested by the low expression level when only the mutant cRNA is injected. When the relative concentration of the mutant cRNA was increased to 1.3, the chance of recording a low conductance channel type was higher, and we recorded the full spectrum of channel populations. Further increase of the ratio of the mutant cRNA to 2 and 4 made the distribution more tilted to the low conductance channel populations. Fitting of a binomial

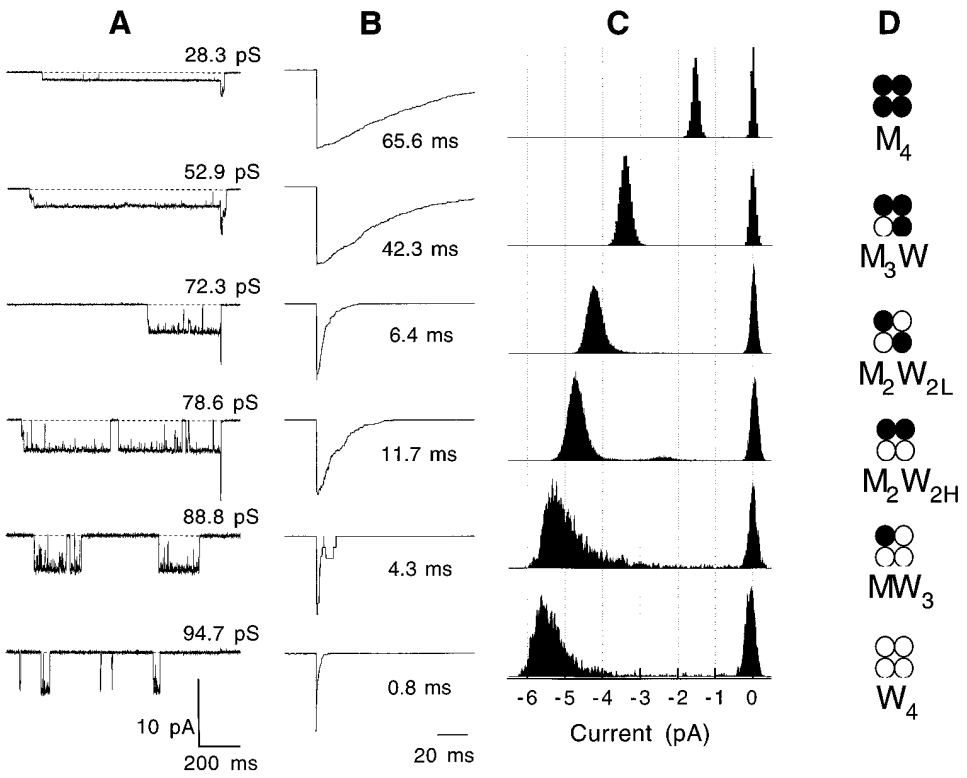

FIGURE 1. Coexpression of WT and mutant cRNAs produces channels with six distinct phenotypes. (*A*) Representative single channel currents, activated by a depolarizing pulse from a −100 mV holding potential to −60 mV, followed by a hyperpolarizing pulse to −140 mV. Dotted lines indicate baselines; currents were filtered at 1 kHz. (*B*) Normalized tail currents at −120 mV were assembled from idealized single channel recordings of each channel type. Given in each panel is the time that the current decays to its half peak amplitude. (*C*) Amplitude histogram of each channel type, measured at −60 mV. The fully open and closed levels are seen as the major peaks; the small intermediate-current components seen in the lower histograms arise from poorly resolved closures and from occasional long-lived dwells in sublevels not related to activation. (*D*) A cartoon illustrating possible combinations of WT and mutant subunits, represented by ○ and ●, respectively, corresponding to the channel phenotypes. M, mutant subunit; W, WT subunit.

distribution to the data yielded satisfactory results (Fig. 2 *B*), and confirmed that five channel populations correspond to distinct stoichiometries.[2]

It should be noted that whatever the cRNA ratio, the probabilities of recording 72.3 and 78.6 pS channels were always similar (Fig. 2 *A*). This is to be expected if these two channel populations reflect the same subunit stoichiometry (M_2W_2) but differ in some other way, for example having different permutations of subunits. In heteromultimeric cyclic nucleotide–gated channels, it has been found that channels with the same stoichiometry but different relative positions of subunits can be distinguished by a large conductance difference (Liu et al., 1996*a*).

To further establish the assignment of the channel stoichiometry, tandem dimer constructs were made in which one copy of the WT cDNA was covalently linked with one copy of the mutant cDNA. These constructs were made with both orientations, M–W and W–M. Single channel recordings from oocytes expressing these tandem dimers showed two main channel populations that belong to the putative M_2W_2 channel types (Table I). Of 44 single channels, we recorded 27 belonging to the 72.3-pS population and 14 belonging to the 78.6-pS population. Three channels were seen that belong to the 52.9-pS population. It is known that tandem constructs do not guarantee the stoichiometry of the assembled channels (McCormack et al., 1992; Hurst et al., 1992, 1995; Yang et al., 1997). However, if we make the usual assumption that the majority of the channels have the correct stoichiometry as defined by the tandem linkage (Isacoff et al., 1990; Liman et al., 1992; Heginbotham and MacKinnon, 1992), these results support the assignment of these intermediate conductance populations to M_2W_2 channels.

Tandem W–W and M–M dimer constructs were also made. When these cRNAs were coinjected, the two intermediate conductance channel populations were observed along with the two homomeric channel populations (Table I). Of the intermediate conductances, 78.6-pS channels were observed much more frequently than the 72.3-pS channels. Together with the other re-

[2]In the fits, it can be seen that the homomultimeric channel types occurred more often than is expected from the binomial distribution. Perhaps there is local enrichment of subunit types in the endoplasmic reticulum as assembly occurs. One speculation is that the existence of polyribosomes on single RNA strands give rise to a local predominance of one subunit species in the endoplasmic reticulum, resulting in a bias toward preferential assembly of homomultimers even when distinct cRNA species are present.

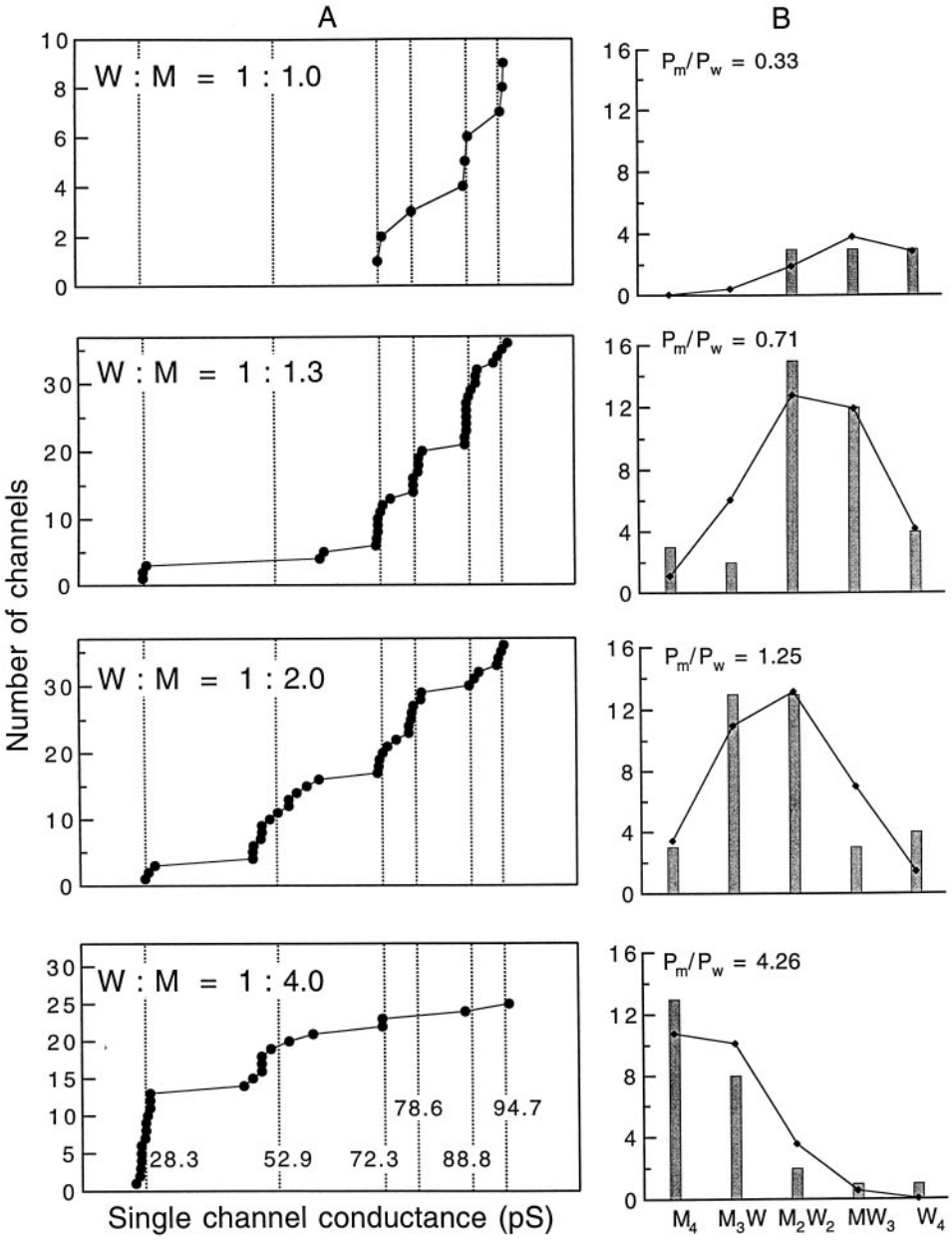

FIGURE 2. Distributions of channel types. (*A*) Cumulative histograms of single channel amplitudes observed in patches from oocytes coinjected with WT and mutant cRNAs at the various ratios (W:M) indicated. Current amplitudes, measured at −60 mV, were taken from fits of the amplitude histograms as shown in Fig. 1 *C* with a mixture of Gaussian functions. Dotted lines indicate the mean of each group, whose value is given in the bottom panel. (*B*) Histograms showing the number of observed channels belonging to each group. The data were fitted to a binomial distribution (*solid lines*) and the probability ratio that generated the maximum likelihood is given as P_m/P_w in each panel.

sults from tandem dimers, this result suggests that the 78.6-pS population represents channels with pairs of like subunits adjacent to each other, while the 72.3-pS channels have like subunits facing each other across the central axis. We shall assume these assignments, which are summarized in Fig. 1 *D*, for the remainder of this paper.

Characterization of Sublevels

We have used an amplitude histogram analysis to detect sublevels in the various channel types. Unlike the threshold-crossing method we previously used to estimate dwell times in the M_4 channels (Zheng and Sigworth, 1997), the amplitude histogram method is less sensitive to noise spikes that, if large enough to cross

TABLE I

Single Channel Populations Recorded from Oocytes Expressing Dimer cRNAs

	Number of channels observed with the given conductance (pS)					
Dimer type	28.3	52.9	72.3	78.6	88.8	94.7
W–M	0	0	14	4	0	0
M–W	0	3	13	10	0	0
M–M/W–W	13	3	2	10	0	3
Apparent stoichiometry	M_4	M_3W	M_2W_{2L}	M_2W_{2H}	MW_3	W_4

Single channel recordings were made in membrane patches having one to five channels. Conductance was calculated from measurements of current steps at −60 mV assuming a linear I-V relation and a reversal potential of 0 mV. The ratio of M–M to W–W dimer cRNA concentration in the coinjection experiments was ~2:1.

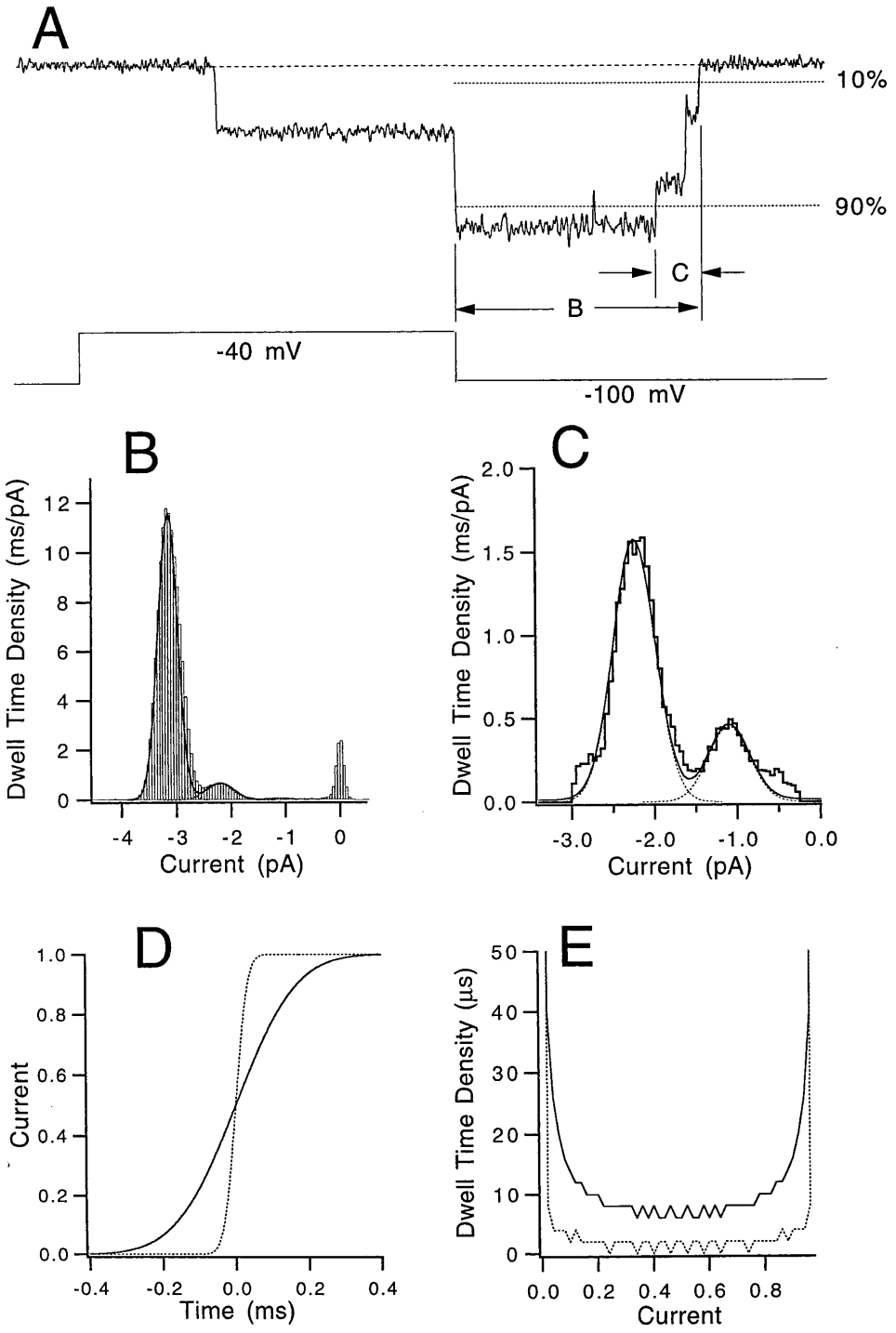

FIGURE 3. Two types of amplitude histograms from tail currents. (*A*) A representative current trace from the M_4 channel. The holding potential was −100 mV. The dashed line indicates zero current level; data were filtered at 1 kHz. Two thresholds (*dotted lines*) were used to detect the times when current crossed 10 and 90% of the fully open current level during deactivation at −100 mV. (*B*) Tail histogram, made by accumulating all the data points in the tail current time course from 148 sweeps, scaled to units of milliseconds per picoampere. Superimposed are Gaussian functions fitted to each peak (*dotted curves*) and their sum (*solid curve*). The peak position of each Gaussian gives an estimate of each current amplitude, and the area under each Gaussian gives an estimate of the mean dwell time of that state. This histogram included sweeps in which the channel failed to deactivate during the 200-ms recording period; thus, the sublevel components are artifactually reduced in area. (*C*) Transition histogram, made by accumulating those data points that fell between the final crossing of the 90% threshold and the subsequent crossing of the 10% threshold. This histogram shows more clearly the dwells in sublevels. (*D*) Simulated current steps of unit amplitude after Gaussian filtering (1 kHz, *solid curve*; 5 kHz, *dotted curve*) show finite dwell times in the transition range. (*E*) Scaled amplitude histograms from the time courses in *D*. Notice that the apparent dwell times from a current step at 1 kHz are much shorter than those obtained from the tail transitions in *C*.

the thresholds, would generate false events. Fig. 3 shows how the two kinds of amplitude histograms were made from single-channel tail currents. Thresholds were used to detect when a channel makes its last transition from the fully open level to the sublevels (the time of crossing the 90% threshold) and from the sublevels to the closed level (the time of crossing the 10% threshold). All the data points in the tail up to the time of crossing the 10% threshold were accumulated in the "tail histogram," which describes the whole tail current time course (Fig. 3 *B*). Only those data points that fell between the 90 and 10% thresholds were accumulated to construct the "transition histogram," which describes dwells in the sublevels (Fig. 3 *C*). Both histograms were accumulated from many sweeps and were scaled to the units of milliseconds per picoampere so that the value of each bin was proportional to the mean dwell time at that current level. The peaks in the histograms repre-

sent stable current levels in single channel recordings, whose position and area give estimates of the mean conductance and the mean lifetime. In the voltage ranges where we used this analysis, the transitions were predominantly unidirectional; the histogram method is expected to overestimate the mean lifetime if multiple dwells in a given state occur during the deactivation time course. In the case shown in Fig. 3, the mean dwell times estimated from the histograms of the open, sub_2, and sub_1 states were 119, 17.7, and 5.4 ms, respectively. Threshold analysis of the same data yielded similar values of the mean dwell times: 80.5, 9.2, and 5.3 ms.

Because of the effect of filtering on the current monitor signal, an instantaneous step transition will appear to have a finite transition rate (Colquhoun and Sigworth, 1995). This will give entries into the above histograms even when a deactivation transition has no dwell in sublevels. We estimated the sensitivity of the amplitude histogram method to this effect by constructing a transition histogram from a step function that had been passed through a Gaussian filter of 1 or 5 kHz bandwidth (Fig. 3 *D*), similar to the case of the single channel recordings. As shown in Fig. 3 *E*, the histograms have very low amplitudes, <10 μs per current unit in most of the 10–90% current amplitude range even when the 1-kHz filter is used. Therefore, we expect that the histogram peaks such as in Fig. 3, *B* and *C*, mostly reflect dwells in stable current levels rather than the time spent during current transitions.

Sublevels Exist in Heteromultimeric and W_4 Channels

We have previously shown that in M_4 channels two sublevels can be identified whose conductances are ~37 and 70% of the fully open current level (Zheng and Sigworth, 1997). Conductances of the sublevels have a linear voltage dependence in the range from −60 to −140 mV. Sublevels are observed during both channel activation and deactivation.

When single channel currents were recorded from the heteromultimeric channels, we found that sublevels also existed. Fig. 4 *A* shows representative tail currents from each channel type. Dwells in the sublevels could be identified in the tail histograms (Fig. 4 *B*) for the slowly deactivating channels and are more readily seen in the transition histograms for every channel type (Fig. 4 *C*). Two sublevels were identified in each channel type. We call the sublevel having a larger conductance sub_2, and the other sub_1, as we did for the M_4 channel sublevels. Similar to those in the M_4 channels, the sublevels are strongly coupled to channel activation. Channel activation usually showed a "staircase" current transition having the closed → sub_1 → sub_2 → open sequence, and the deactivation showed the reverse sequence. Also like the M_4 channel sublevels, the sub_2 sublevels in heteromultimeric channels had longer lifetimes compared with the sub_1 sublevels, as shown by a larger sub_2 peak in most transition histograms. In the case of M_2W_2 channels, an extra sublevel having the smallest conductance was also observed. We call it sub_2' because its kinetics are most similar to sub_2; it has no counterpart in other channel types, but was seen in both the 72.3- (M_2W_{2L}) and 78.6-pS (M_2W_{2H}) channels.

Staircase current transitions were not obvious in W_4 single channel traces, and no sublevel peaks were visible in the tail histogram. But when the transition histogram was constructed, two peaks similar to those in the other channel types were observed. Sublevels could occasionally be seen in the deactivation time course of W_4 channels, such as the one shown in the bottom panel of Fig. 4 *A*.

With the nearly symmetrical K^+ solutions used, both the fully open state and the sublevels were found to have linear I-V relationships within the voltage range studied (−60 to −140 mV; narrower voltage ranges were used for the MW_3 and W_4 channels). The current amplitudes at −100 mV are listed in Table II. The slope conductances of the sub_2 sublevels are 54–70% of the fully open level; those of sub_1 are 23–44%. Mean lifetimes of the open level and the sublevels were estimated from histogram fits and are plotted in Fig. 5. It can be seen that both the open times and the dwell times in the sublevels decrease with each additional WT subunit. The mean lifetimes of sub_2 and sub_1 sublevels in the W_4 channels at −100 mV were estimated to be 280 and 70 μs, respectively. The short lifetimes, in addition to the presence of frequent brief closures from the open state, made the sublevels in the W_4 channels not readily observable.

Our previous study of the gating kinetics of the M_4 channel showed that the lifetimes of the open level and sublevels are all voltage dependent. The lifetime of the open level is mainly determined by the voltage-dependent backward transition that becomes slower at more depolarized voltages. The lifetimes of the two sublevels, on the other hand, are determined by both forward and backward transitions. The voltage dependence of these transitions gives rise to a bell-shaped lifetime curve in each sublevel with a peak around −100 mV. In the heteromultimeric and W_4 channels, the lifetimes exhibit very similar voltage dependences (Fig. 5). The main open time is always longer at more depolarized voltages, and the lifetime in each of the sublevels peaks around −100 mV.

Sublevels in the Various Channel Types Show Similar Kinetic Behaviors

Besides the above-stated similarities among sublevels in different channel types, we also tested other gating properties. One feature that is characteristic for the M_4 channel sublevels is the strong coupling between the

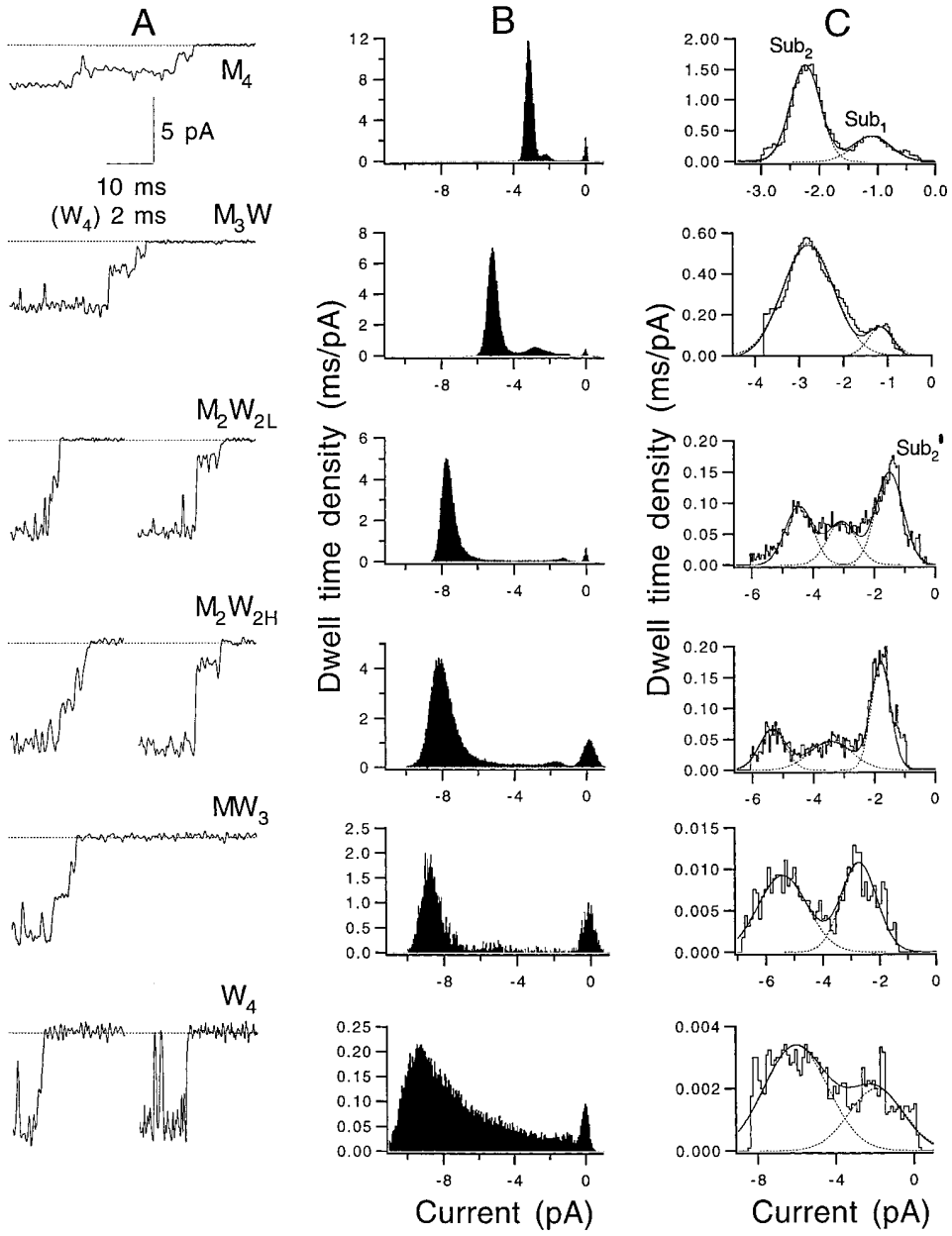

FIGURE 4. Sublevels in each channel type. (*A*) Representative single-channel deactivation time courses at −100 mV. The repolarization to −100 mV preceded the beginning of each trace, which shows only the vicinity of the recording where the deactivation transition occurred. Dotted lines indicate baselines. Data were filtered at 1 kHz except for W_4, which was filtered at 5 kHz. Two sweeps from a M_2W_{2L} channel and two sweeps from a M_2W_{2H} channel are shown to demonstrate two types of closing transitions, one through sub_2 and sub_1, the other through sub_2'. Two W_4 sweeps are also presented (with expanded time scale as shown). The left sweep shows a transition with an obvious dwell in sub_2, the right sweep has no apparent dwells in sublevels. (*B*) Tail histograms at −100 mV, from 148 (M_4), 223 (M_3W), 298 (M_2W_{2L}), 165 (M_2W_{2H}), 40 (MW_3), and 412 (W_4) sweeps, respectively. (*C*) The corresponding transition histograms, obtained as in Fig. 3 *C*. Thresholds defining the transitions were 10 and 90% except in the case of W_4, where the thresholds were set at 15 and 85% of the fully open current amplitude.

open level and the sublevels. It was found in the previous study that an activating channel always traverses the sub_2 sublevel before it reaches the final open level. Deactivation also always passes through the sub_2 sublevel. It is harder to carry out the same test in the heteromultimeric and W_4 channels due to the shorter lifetimes of their sublevels. However, we did a less stringent test by asking whether the channel has to traverse at least one sublevel during deactivation.

Evidence for traversal of sublevels comes from the "excess time" measured in the single channel closing time course at −100 mV using two thresholds, 10 and 90% in amplitude. If a channel closes directly from the fully open to the closed level, a finite dwell time will be measured due to the filter rise time. Because the

TABLE II

Comparison of Single Channel Currents with K^+ or Rb^+ as the Current Carrier

	i_K			i_{Rb}		
Channel type	Open	Sub_2	Sub_1	Open	Sub_2	Sub_1
	pA			*pA*		
M_4	3.2	2.2	1.1	5.0	2.0	0.5
M_3W	5.2	2.8	1.2			
M_2W_{2L}	7.8	4.8	3.4	4.1	2.0	1.2
M_2W_{2H}	8.1	5.3	3.4			
MW_3	8.8	5.4	2.7			
W_4	9.5	5.9	2.6	2.4	0.9	—

Current amplitude was estimated at −100 mV from amplitude histograms. The pipette solution contained 140 mM of the test ion.

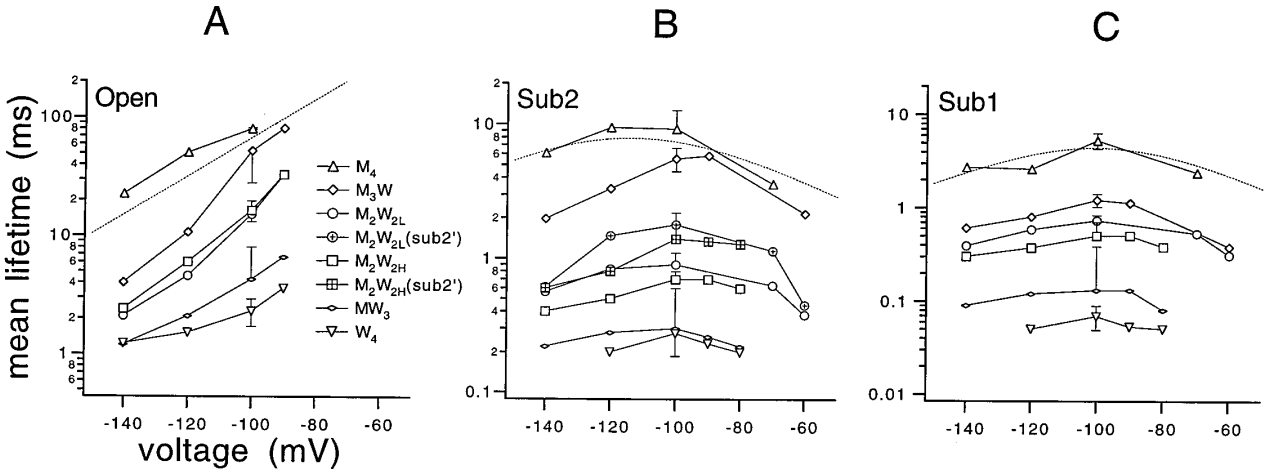

FIGURE 5. Voltage dependence of the mean lifetimes in each current level. Mean dwell times of the open (*A*), sub_2 (*B*), and sub_1 (*C*) states were estimated from Gaussian fits to transition histograms as in Fig. 4. Mean dwell times for the M_4 channel were measured by threshold analysis (Zheng and Sigworth, 1997); the histogram analysis of M_4 currents yielded similar results. The standard deviations are also shown for each channel type at −100 mV. The numbers of channels measured for each channel type are: W_4, $n = 2$; MW_3, $n = 5$; M_2W_{2L}, $n = 4$; M_2W_{2H}, $n = 3$; MW_3, $n = 2$; W_4, $n = 2$. The dotted curve in each panel represents the prediction from the kinetic scheme for the M_4 channel given by Zheng and Sigworth (1997). The brief lifetimes of sublevels in MW_3 and W_4 channels precluded their measurement at voltages below −120 and above −80 mV.

threshold-crossing time is perturbed by the Gaussian background noise, the measured dwell times will have an approximately Gaussian probability density $f_0(s)$ (see Eq. 5). Alternatively, deactivation that traverses sublevels will have the approximate probability density $f_1(s)$ (given by Eq. 6) that is a weighted sum of one or two exponential functions (corresponding to the lifetime of each sublevel) convolved with a Gaussian function. We assumed that a closure could be either a direct transition or one traversing sublevels. Each individual measurement of the transition time was thus fitted with

$$f(s) = A_0 f_0(s) + (1 - A_0) f_1(s) , \qquad (7)$$

and the factor, along with the other parameters, was adjusted to generate the best fit to a set of 60–943 measurements. The value of A_0 gave an estimate of how many transitions were direct transitions that avoided traversing sublevels. We chose a test potential of −100 mV because under this condition the sublevels exhibit the longest lifetimes. Fig. 6 shows a histogram of the measured transition times during deactivation for each channel type, and the probability density function that yields the maximum-likelihood fit. It was found that, for the M_4 channel, <10% of the transitions could be described by direct transitions, consistent with the channel always traversing at least one sublevel. Similarly, all the heteromultimeric channels and the W_4 channel had the majority of the measured transitions (>80% in each case) being accounted for by the exponential term(s). Thus, we conclude that all these channel types deactivate through sublevel states.

Our previous study of the mutant channel showed that its activation can take two alternative paths from closed to the final open level. One path is through both sub_1 and sub_2; the other is directly from closed to sub_2. This generates nonzero dwells in sub_2 but a substantial population of zero dwells in sub_1. We tested to see whether the sublevels in the other channel types also show similar correlation. The dwell time in each sublevel was measured during the activation time course at −60 mV by using three thresholds. (This analysis could not be applied to the W_4 channel because of its very brief transition times.) Under these conditions, we indeed observed activation time courses in each channel type that contained substantial dwells in both sub_2 and sub_1 sublevels (Fig. 7), suggesting that the activation of these channels may follow the same pathways as the M_4 channel. However, dwells in the smallest sublevel found in M_2W_{2L} channels, sub_2', shows a negative correlation with dwells in the other two sublevels. Of 167 sweeps, there were only 2 for which activation showed nonzero dwells in both the sub_2' and in the sub_1/sub_2 current ranges. Activation of a single M_2W_{2L} channel thus seems to show two alternative paths: one proceeds through sub_1 and sub_2 like the mutant channel, while the other path passes only through the sub_2' state. One example of each alternative is presented in the M_2W_{2L} panel of Fig. 4 *A*. Also shown in the figure is the same behavior that was seen in M_2W_{2H} channels.

In conclusion, the sublevels in all channel types show a similar gating pattern, with the exception of the M_2W_2 channels, which seem to gate through alternative

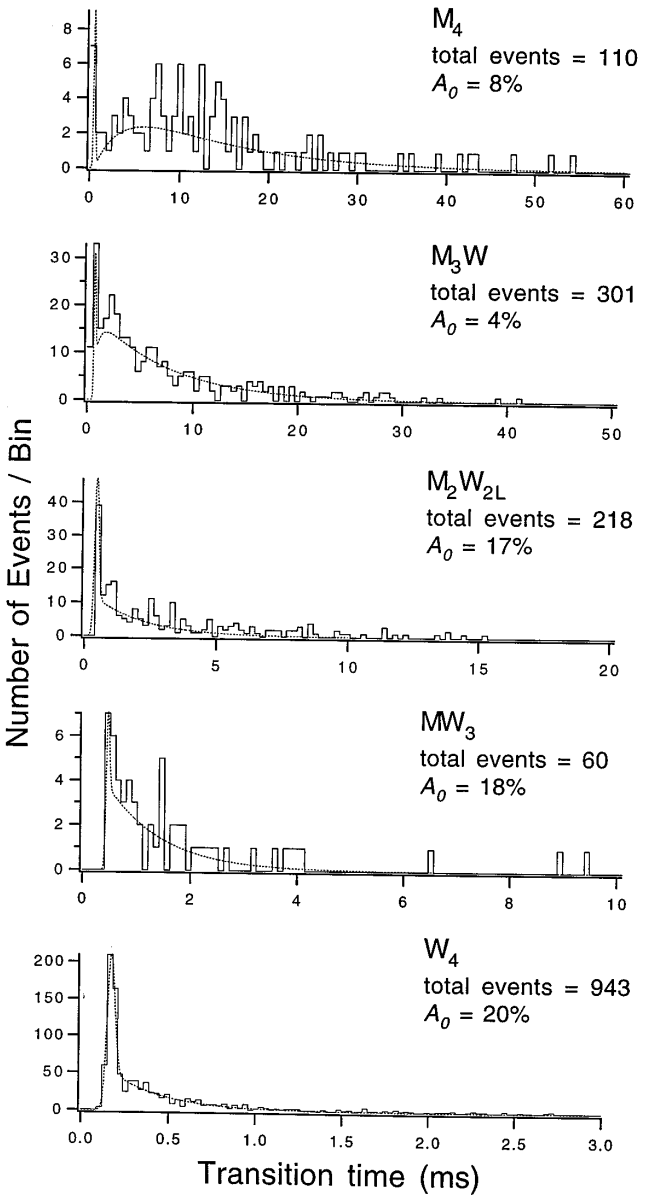

FIGURE 6. Closing transitions at −100 mV are characterized by the time the final transition spent between 90 and 10% of the current amplitude. Superimposed on the histograms are results of maximum-likelihood fits to each measured value assuming that the closures are either instantaneous transitions from fully open current to zero current level (whose measured dwells are approximated by a Gaussian distribution, Eq. 5) or transitions through one (for M_2W_{2L}, MW_3, and W_4) or two (for M_4 and M_3W) sublevels, whose measured dwells are approximated by one or two exponential distributions convolved with a Gaussian probability density function with the same variance (Eq. 6). The time constant of the exponential functions and the fraction A_0 of the instantaneous component are: M_4, τ_1 = 12.1 ms, τ_2 = 3.2 ms, 8%; M_3W, τ_1 = 6.9 ms, τ_2 = 0.9 ms, 4%; M_2W_{2L}, τ = 3.6 ms, 17%; MW_3, τ = 1.1 ms, 18%; W_4, τ = 0.26 ms, 20%.

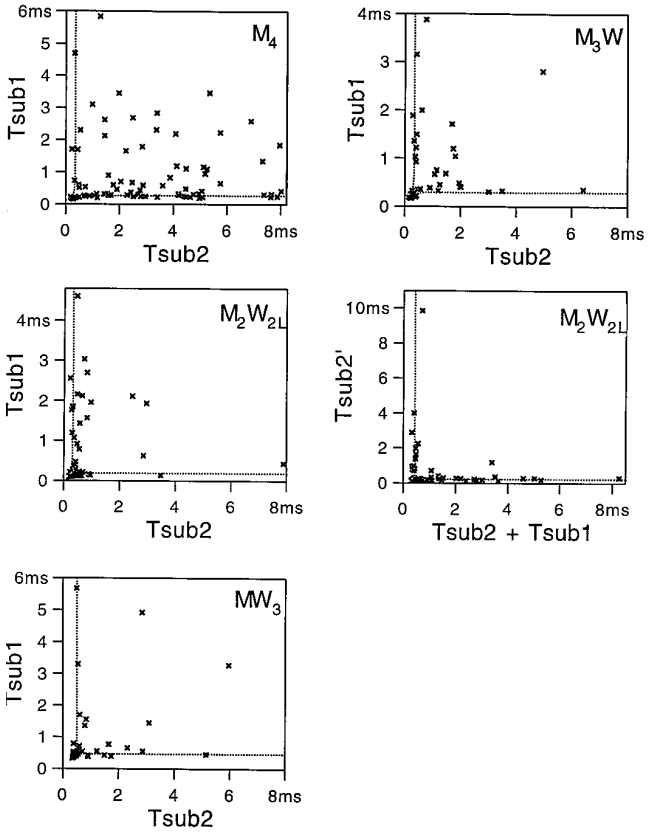

FIGURE 7. Correlation of dwell times in sublevels. Activation transitions at −60 mV were filtered at 1 kHz and dwells in each sublevel were measured by a pair of thresholds that bracketed it. Only those sweeps showing a unidirectional progression of conductance levels were counted. Each plotted point represents the apparent dwell times in sub_1 and sub_2, except in the right-hand M_2W_{2L} graph where dwells in sub_2' are plotted against the total time spent in the two larger sublevels. In each graph, the dotted curves represent the locus of points obtained from simulations in which one or the other sublevel is skipped during activation. In all channel types, there were many transitions having nonzero dwells in both current levels, except for the M_2W_{2L} channel, for which only 2 of 167 deactivations showed a long dwell in both the sub_2–sub_1 level and the sub_2' level. The M_2W_{2H} channels behaved similarly to the M_2W_{2L} channels (data not shown).

paths. The likely explanation for the similarity is that the sublevels represent the same gating process that is preserved in all the channel types.

Sublevels Have Differing Ion Selectivities

It has been previously found that the various conductance levels in the mutant channels have differing ion selectivities (Zheng and Sigworth, 1997). At −100 mV, the amplitude ratio of Rb^+ to K^+ current changes from 1.55 in the open state to 0.90 in the sub_2 state, and 0.47 in the sub_1 state. We were interested in testing whether the sublevels in heteromultimeric and W_4 channels also show similar selectivity differences. K^+ in the pipette was replaced with Rb^+ in recordings using inside-out

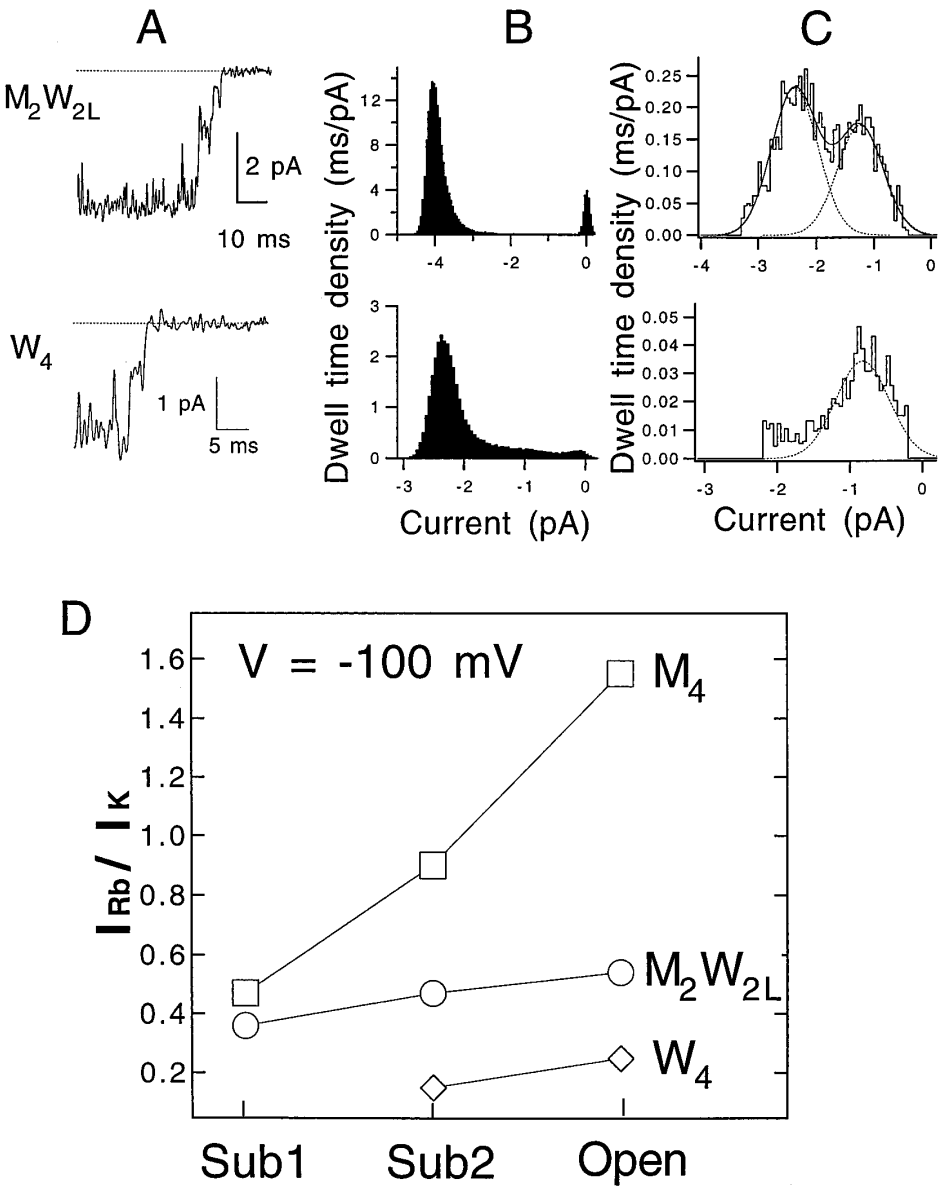

FIGURE 8. Current amplitudes with Rb^+ ion as the charge carrier. (*A*) Representative tail currents of M_2W_{2L} (*top*) and W_4 (*bottom*) channels recorded at −100 mV with 140 mM Rb^+ ion in the pipette solution. (*B*) Tail histograms of M_2W_{2L} and W_4 channels. (*C*) Transition histograms accumulated from the final closing transitions. The two peaks in the M_2W_{2L} histogram have areas of 5.0 and 3.1 ms, respectively. The peak in the W_4 histogram has an area of 0.6 ms. (*D*) Ratio of Rb^+ to K^+ current amplitudes in the fully open level and in sublevels, measured at −100 mV.

patches, and the inward Rb^+ currents were recorded at −100 mV. As shown in Fig. 8 *A*, both M_2W_{2L} and W_4 channels showed sublevels in Rb^+ currents. We identified two sublevels in M_2W_{2L} channel currents that were similar to the sub_2 and sub_1 sublevel in K^+ currents. We could identify only one sublevel in W_4 Rb^+ currents that resembled the sub_2 sublevel, though it is quite possible that an additional sublevel exists but was indistinguishable from the baseline current. The Rb^+ ion seems to stabilize the conducting states, as suggested by the 3–10-fold longer lifetimes of both the open and the sublevel states (Fig. 8 *A*). The longer lifetimes are reflected in the histograms in Fig. 8, *B* and *C*, as components with larger areas.

In the M_4 channel, the Rb^+ current is larger than the K^+ current in the open level but smaller than the K^+ current in each sublevel. In contrast, the M_2W_{2L} and W_4 channels have Rb^+ currents that are smaller than the K^+ currents in all current levels (Table II). The Rb^+ to K^+ current ratio for the open level was found to be larger than that for each sublevel of the M_2W_{2L} channels and for sub_2 in the W_4 channels (Fig. 8 *D*). Thus, in all three channel types, the sublevels tend to exclude the larger Rb^+ ion.

DISCUSSION

We have previously reported sublevels in T442S mutant *Shaker* channels that apparently represent intermediate conformations during voltage-dependent activation (Zheng and Sigworth, 1997). This paper extends the study to heteromultimeric channels containing one to

three mutant subunits as well as channels with no mutant subunits. It is found that sublevels with similar kinetic and permeation properties exist in all these channel types, consistent with the idea that the T442S mutation changes the free energies of some conformational states, but does not introduce new states. Each mutant subunit is seen to contribute to the stabilization of the conducting states by approximately the same amount. In addition, the magnitude of this effect is essentially equal in the open level and in each of the two sublevels. Consistent with earlier results on the mutant channel, it is found that sublevels in one heteromultimeric channel type and in the W_4 channel have ion selectivities that differ from that of the fully open level.

Stoichiometries of Heteromultimeric Channels

Heteromultimeric channels were made by coexpression of the WT and mutant subunits and also by using tandem dimer constructs. To identify the subunit stoichiometry, we made use of the large difference in kinetics and conductance between the two homomultimeric channel types. Several lines of evidence supported our assignment of the stoichiometries. (*a*) Coexpression gave rise to six channel populations with distinct single channel conductances; the largest conductance was identical to the W_4 channel and the smallest one was identical to the M_4 channel. (*b*) Parallel to the conductance differences, each channel population showed distinct kinetic properties. Channels with higher conductance had shorter mean open times, fast tail currents, and many brief closures. Changes in the mean lifetimes of the sublevels also followed the same trend. (*c*) In the coexpression experiments, the distribution of channel populations varied as the ratio of WT to mutant cRNA was changed, such that as more WT cRNA was injected the chance to record a channel with higher conductance was increased. (*d*) The relative probability of observing two intermediate populations showed no variation with changes in the cRNA ratio, suggesting that these populations represent the same subunit stoichiometry. (*e*) Expression of tandem dimeric constructs allowed the assignment of the two intermediate populations. Like the result obtained by Liu et al. (1996*a*) in the case of cyclic nucleotide–gated channels, channels formed by pairs of adjacent WT or mutant subunits were seen to have a higher conductance than those formed by alternating subunit types.

Sublevels in Heteromultimeric Channels and W_4 Channels

In our previous study (Zheng and Sigworth, 1997), we found that the T442S mutation greatly increases the channel open time while leaving the first latency to opening unchanged. We concluded that the T442S mutation preserves the activation conformational changes but lowers the free energy of the open conformation; by doing so, it also makes short-lived intermediate subconductance states readily visible. If this is the case, one expects that sublevels will persist when the stabilizing effect of the T442S mutation is gradually reduced by replacing each mutant subunit with the WT subunit. Indeed, sublevels are seen with progressively shorter lifetimes, reflecting these states becoming more and more unstable, as the number of mutant subunits was decreased. Despite the differences in lifetimes, sublevels in the various channel types show several common properties. First, the lifetimes in each sublevel show similar voltage dependence, peaking at ~ -100 mV and becoming shorter at more depolarized and hyperpolarized voltages. Second, deactivation in each type of channel nearly always traverses at least one sublevel. Third, it was observed that the sublevels and the open level have differing ion selectivity. The similarities in the gating and permeation properties of these sublevels strongly suggest that they represent the same conformational states preserved among the channel types.

It should be noted that the M_2W_2 channels show an additional sublevel, which we have called sub_2'. Its appearance is negatively correlated with any dwell time in the usual sub_1 and sub_2 states (Fig. 7), and therefore represents an alternative pathway for channel deactivation in this channel type.

Do Activation-coupled Sublevels Exist in Shaker Channels?

Subconductance states have been observed in many channel types (for review see Fox, 1987). Activation-coupled sublevels like the ones studied here have been reported in other members of the voltage-gated potassium channel superfamily, such as the rat muscle calcium-activated K^+ channel (Ferguson et al., 1993) and the rat Kv2.1 channel. Chapman et al. (1997) have demonstrated activation-coupled sublevels not only in wild-type Kv2.1 but also in two mutant channels that make the sublevels more visible. The W_4 channel used in our study is a chimeric *Shaker* channel whose S6 segment is transplanted from Kv3.1 (also known as NGK2). The W_4 channel shows gating behavior quite similar to the wild-type *Shaker* channel, though its conductance is fourfold larger (Lopez at al., 1994). However, the difference in sequence raises the question of whether wild-type *Shaker* channels would also open through the same sublevels.

The smaller conductance and flickering channel openings make it practically impossible to detect sublevels in *Shaker* channels. However, the data from related channels could provide some indirect evidence. Previously, we studied a channel with the T442S mutation in the NH_2-terminal-truncated *Shaker* channel background (which we called SS; Zheng and Sigworth, 1997). This channel showed prolonged channel open-

ings and two activation-coupled sublevels like the M_4 channel in this study. The relationship of *Shaker*, SS, and the channels we studied here are described in Scheme I.

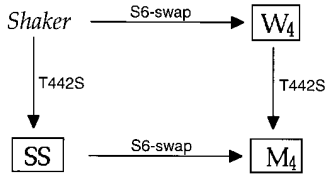

(SCHEME I)

Channels in the lower row were generated by introducing the T442S mutation; channels at the right hand side were generated by introducing the Kv3.1 S6 region. Activation-coupled sublevels have now been found in SS, M_4, and W_4 channels (indicated by boxes). The fact that the S6 swap and the T442S mutation by themselves did not generate or eliminate the sublevel phenomena thus argues for the existence of sublevels in *Shaker* channels. In our W_4 channel, the maximal lifetimes of sub_2 and sub_1 are estimated to be 280 and 70 μs, respectively. If the *Shaker* channel sublevels have the same lifetimes, they will not be easily detected by conventional methods.

It should be noted that sublevels of a different kinetic nature are seen in wild-type *Shaker* channels (Hoshi et al., 1994; Zheng and Sigworth, 1997). It has been estimated by Schoppa and Sigworth (1998*a*) that NH_2-terminal-truncated *Shaker* channels spend 17% of the open time in conductance levels below the main level. These sublevels do not seem to be activation coupled, but rather occur randomly throughout the recording (see Fig. 2 *B* in Zheng and Sigworth, 1997). A transition to this kind of sublevel would contaminate our measurement of activation-coupled sublevel lifetimes if it were to occur close in time to the final closing transition. Such contamination may explain the slower exponential component that was seen in the W_4 channel deactivation time course (Fig. 6).

Subunit Effects on Dwell Times Suggest Concerted Steps

The main kinetic effect of the T442S mutation was previously found to be the stabilization of the open conformation (Zheng and Sigworth, 1997). However, depending on the presumed mechanism of subunit interaction, the stabilization effect of each mutant subunit on the lifetimes of the open level and of the sublevels could be quite different. We consider here two extreme possibilities. In the first mechanism, each subunit is assumed to independently undergo voltage-dependent transitions that are equivalent but proceed at different rates in mutant and WT subunits. The scheme of Zagotta et al. (1994*b*) is of this form, and has an open state that consists of all four subunits being in the permissive state S_2 (see Scheme II).

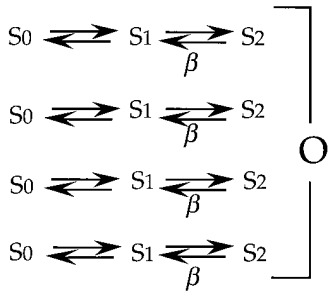

(SCHEME II)

According to Scheme II, the lifetime τ_o of the open state is determined by

$$\tau_0^{-1} = n\beta_m + (4-n)\beta_w , \qquad (8)$$

in which β_m and β_w are rate constants of the mutant and WT subunits, respectively, and n is the number of mutant subunits in the channel. Thus, each subunit has an additive effect on the rate of transition. Our previous study has shown that β_m is two to three orders of magnitude larger than β_w. The prediction of Eq. 8 therefore is that the lifetime of the open state will show a large difference between the M_4 and the M_3W channel, but show much smaller differences as the number of mutant subunits further decreases.

In the second mechanism, the subunits make concerted transitions in the final opening steps; an example is Scheme III, in which the final two transitions are concerted.

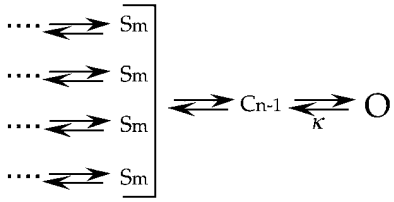

(SCHEME III)

Because they are forced to undergo the transitions simultaneously, the subunits have an additive effect on the free energy change of the concerted transitions. Thus, the lifetime of the open state will depend exponentially on the number of mutant subunits,

$$\tau_0^{-1} = \kappa = Ae^{-[n\Delta G_m^* + (4-n)\Delta G_w^*]/kT} , \qquad (9)$$

in which ΔG_m^* and ΔG_w^* are the free energy contributions to the closing rate constant κ from a single mutant or WT subunit, respectively. The concerted transition mechanism predicts that each subunit affects the lifetime by the same factor.

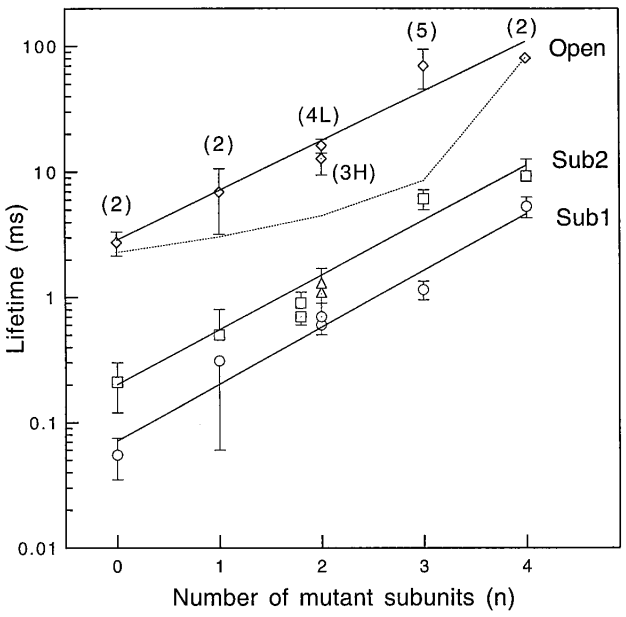

FIGURE 9. Mean lifetime of each current level depends on the number of mutant subunits. The number of channels measured is given in parentheses. Values from M_2W_{2H} channels are presented as dotted symbols to distinguish them from those of M_2W_{2L} channels; for these two channel types, the sub_2' dwells are also plotted (△). Solid lines are fits to the lifetimes at −100 mV of an exponential function in which n is the number of mutant subunits as expected from Eq. 9. The k values are 0.90 (*Open*), 1.01 (*Sub2*), and 1.04 (*Sub1*). The dotted line represents the predicted lifetime of the open state assuming that each subunit undergoes independent transitions (Eq. 8). In this case, the transition rates (β_m and β_w) of mutant and WT subunits were taken from the mean open time ($\bar{t}$) of the corresponding homomultimeric channels as $\beta_x = 1/(4\bar{t}_x)$.

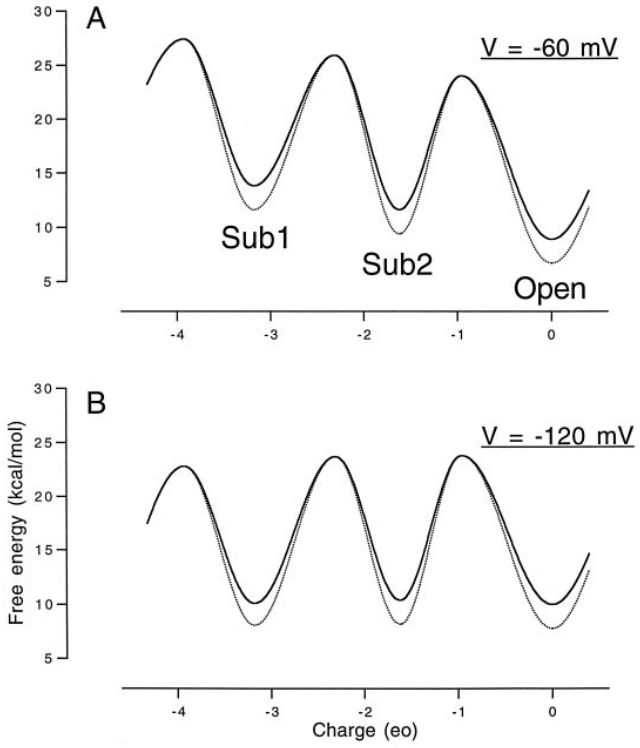

FIGURE 10. Hypothetical free energy profiles for M_4 (*solid curve*) and W_4 channels (*dotted curve*), drawn with gating charge movement as the reaction coordinate. (*A*) Energy profile during channel activation at −60 mV. (*B*) Energy profile during deactivation at −120 mV. The free energy change for each transition and the associated charge were calculated from the kinetic model of M_4 channels (Zheng and Sigworth, 1997). The free energy differences between M_4 and W_4 channels were calculated from the mean lifetimes of each state. The free energy at transition states was taken to be the same between M_4 and W_4 for simplicity, and because the entry into conducting states (the first latency) is essentially unaffected by the mutation (Zheng and Sigworth, 1997).

The observed dependence of the conducting state lifetimes on channel stoichiometry is illustrated in Fig. 9. The lifetime in the open level increases by a factor of ∼2.5 with the addition of each mutant subunit. The sublevel lifetimes change in a parallel manner. That the lifetimes appear to change geometrically with the number of mutant subunits is consistent with the concerted transition mechanism as in Scheme III. The independent transition mechanism as in Scheme II predicts very poorly the dependence of the lifetime on the subunit composition; this is illustrated in the case of the open state lifetimes by the dotted lines in Fig. 9.

The slopes of the fitted lines in Fig. 9 correspond to a subunit difference in the free energy change $\Delta G_w^* - \Delta G_m^*$ of ∼0.5 kcal/mol for transitions out of the open level; nearly the same value obtains for transitions from each of the two sublevels. The parallel changes in the stabilities of the three conducting states is illustrated in Fig. 10, which summarizes the kinetic data from our previous study and the present one. It presents hypothetical free energy profiles for the M_4 and W_4 channels, plotted with the gating charge movement as the reaction coordinate. In the energy profiles, the barrier peaks between sub_1 and sub_2 and between sub_2 and the open state are presented as equal in each channel type. The only difference between the W_4 channel and the mutant channel is then that the energy wells are deeper for the mutant channel.

Subunit Transitions Explain Sublevel Kinetics

Shaker channel activation involves many voltage-dependent kinetic transitions (Sigworth, 1994). To describe *Shaker* channel activation, Zagotta et al. (1994*b*) proposed a state topology in which each of the four subunits undergoes two conformational transitions. The channel is taken to be open only when all four subunits are in the open state. To explain the sublevel phenomena of the wild-type Kv2.1 channel and two mutants, Chapman et al. (1997) used a scheme with similar topology but proposed that a partially conducting pore may result when one or more subunits are in the

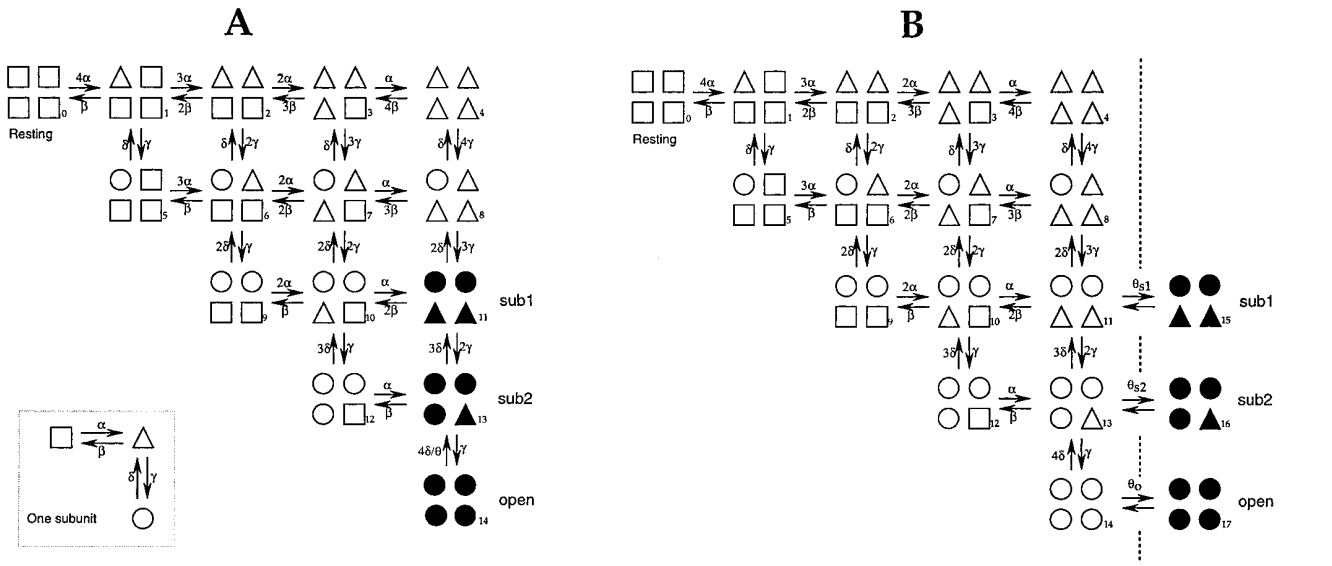

FIGURE 11. Two activation gating schemes. (*A*) The scheme of Zagotta et al. (1994*b*) is shown, in which a single subunit undergoes two voltage-dependent conformational transitions (*inset*) to reach a permissive state (○ and ●). Subunit transitions occur independently, with the exception of a slowed transition from the open state 14 to state 13. The scheme has been modified to identify sublevels sub_1 and sub_2 with states in which two or three subunits are in the permissive state. (*B*) The scheme is modified to include a distinct transition (*dotted line*) that follows activation of the subunits. This allosteric transition is assumed to switch between nonconducting states and open states having different conductances. The equilibrium constants θ_{s1}, θ_{s2}, and θ_o are greatly increased by the T442S mutation. In both schemes, the conducting states are represented by ● and ▲.

"open" conformation. The behavior of the M_4 channel sublevels can also be described by a scheme of this kind (Fig. 11 *A*), which, like Scheme II, assumes that the final transitions before channel opening arise as transitions in individual subunits. This model is sufficient to explain the following three observations from M_4 channels. First, channel activation can occur without a dwell in sub_1 but always traverses the sub_2 sublevel. In the scheme of Fig. 11 *A,* the channel may or may not pass through state 11, but must always traverse state 13, in which three subunits are in their open conformation, before entering the open state. Second, the charge movements associated with the $sub_1 \leftrightarrow sub_2$ and the $sub_2 \leftrightarrow$ open transitions are essentially equal, consistent with their being identical transitions occurring in separate subunits. Third, the three conducting states have differing selectivities. This is easily explained by having distinct open states (Fig. 11 *A,* ● and ▲) that arise from different conformations of subunits.

In the present study, we find that sublevels in the heteromultimeric and W_4 channels appear to have properties that are similar to those of the M_4 channel. Thus, we conclude that the scheme of Fig. 11 *A* can describe the sublevel kinetics of heteromultimeric and W_4 channels as well.

Subunit Transitions or Concerted Transitions?

We are now confronted with a paradox: as we have seen, the stoichiometry dependence of dwell times is best explained by invoking concerted transitions leading to the conducting states of the channel (Fig. 9 and Scheme III); on the other hand, the sublevel kinetics are well described by an independent-subunit model, as in Fig. 11 *A*. Another, surprising observation is that for each of the three conducting states the magnitude of energetic stabilization by mutant subunits is nearly the same (Fig. 10). How can these arguments be reconciled? One possible answer is illustrated by the scheme in Fig. 11 *B*. Again, we assume that there are three open states of the channel having different conductances and selectivities, but in this scheme a final, rapid, forwardly biased transition (indicated by the dotted line) divides nonconducting from conducting states. The dwell times of the channel in the nonconducting states (states 11, 13, and 14) are assumed to be brief compared with the dwell times in the corresponding open states, too brief to be experimentally observed. The forwardly biased equilibria therefore lengthen the observed dwell times (actually the burst durations) in the conducting states by factors equal to the equilibrium constants θ_{s1}, θ_{s2}, and θ_o. We assume that θ_o and θ_{s2} are larger than unity in the W_4 channel, and that all three equilibrium constants increase as the number of mutant subunits increases.

The equilibrium constant θ_o serves the same role as the parameter θ in the model of Zagotta et al. (1994*b*), which suggests a coupling between the final voltage-

dependent transition and the opening of the channel. In the model, the lifetime of the open state of the channel is prolonged by the factor $\theta \approx 10$, and a degree of positive cooperativity is conferred on the activation process. The final transition shown in Fig. 11 *B* has the same effect of lengthening the dwell time in the open state, but also lengthens the dwell times in the sublevels by the same factor.

It should be kept in mind that the model shown in Fig. 11 *B* fails to account for many phenomena, and is presented here only as a tentative hypothesis. Most importantly, it does not account for the alternate activation pathway that involves the sub_2' state. Such a pathway would be expected to arise if an individual subunit's transition rates do depend on the presence of the T442S mutation; as it is, the model assumes kinetic symmetry for simplicity. Also, the underlying scheme of Zagotta et al. (1994*b*) is insufficient to account for kinetic phenomena at voltage extremes, and a more complex model is implicated (Schoppa and Sigworth, 1998*b*). Nevertheless, we prefer to use this simple model for illustrative purposes.

Multiple Activation Gates in the Shaker Channel

It is commonly accepted that *Shaker* channels have at least three gates. The first is responsible for the N-type inactivation process, in which the inner mouth of the channel is occluded by a domain formed by the NH_2-terminal region of each subunit (Hoshi et al., 1990). The second is the C-type inactivation gate, whose behavior is sensitive to ion binding and to mutations at the external mouth of the channel and whose closing is accompanied by motions of residues in that region (Hoshi et al., 1991; Lopez-Barneo and Aldrich, 1993; Liu et al., 1996*b*). When this gate is "closed," the channel can conduct ions but with greatly altered selectivity (Starkus et al., 1997). A related "P-type" inactivation mechanism has been described that also involves residues near the external mouth (DeBiasi et al., 1993*b*; Olcese et al., 1997; Yang et al., 1997). Third, there is the main "activation gate" of the channel, which has been mapped by changes in cysteine accessibility to lie at the intracellular end of the S6 helices (Liu et al., 1997). In the structure of the *Streptomyces lividans* potassium channel (KcsA), the corresponding "inner helices" are seen to form a bundle that has a constriction in this region (Doyle et al., 1998).

Traditionally, the channel gating and selectivity functions have been considered as separate structures in a voltage-gated channel (Hille, 1992). However, the large gating effects of some mutations suggest that the selectivity filter region may also participate in voltage-dependent gating (see, for example, Yool and Schwarz, 1991; Heginbotham et al., 1992; Kirsch et al., 1992; De Biasi et al., 1993*a*, 1993*b*; for review see Sigworth, 1994). The activation-coupled subconductance behavior observed by Chapman et al. (1997) and in our previous study suggest that voltage-dependent processes in individual subunits affect ion permeation. The *Shaker* T442 residue corresponds to T75 in the KcsA channel, which lies at the inner end of the selectivity filter loop. The carbonyl and hydroxyl oxygens of T75 help form the inner ion binding site; it is therefore not surprising that mutations at T442 change the conductance and selectivity of *Shaker* channels. That mutations at T442 also affect the lifetimes of conducting states suggest that the environment of this residue is influenced by the state of the main activation gate; energetic changes due to the mutation would then be mirrored in changes of the open–closed equilibrium of the activation gate.

The results of the present study lead us reluctantly to suggest the existence of yet another gate in the *Shaker* channel. (Here we use the term "gate" in the general sense of a region of the channel complex that, through conformational changes, modulates the ion flux.) This "pore gate" would be responsible for switching among the various conductance levels; the most plausible locus for this gate would be at the selectivity filter, where very small atomic motions would have large effects on conductance and selectivity. In the context of Fig. 11 *B*, we would associate the pore gate with the vertical transitions among the final closed states (states 11, 13, and 14). Its intermediate degrees of opening can be imagined to arise from heteromeric pore conformations, as proposed by Chapman et al. (1997). The allosteric transitions in the scheme are then the transitions of the "main gate" composed of the S6 helix bundle. Voltage-dependent opening of the main gate would be driven by the allosteric equilibrium constants, which increase in the order $\theta_{s1} < \theta_{s2} < \theta_o$, reflecting coupling between the conformational changes that drive the pore gate and the energetics of main-gate opening.

This view of two coupled activation gates, one in the selectivity-filter region and the other at the intracellular end of the S6 helices, is only speculative, but it finds some support from three arguments. First, the existence of two activation gates predicts that a class of direct channel closures, due to closing of the main gate, should exist along with the closures through sublevels that are predominantly seen. A class of weakly voltage-dependent, direct closures is in fact observed in mutant channels. These closures (see Figs. 7 and 9 of Zheng and Sigworth, 1997) are kinetically distinct from the highly voltage-dependent transitions through the sublevels. A second argument involves the C-type inactivation process. This process derives its voltage dependence from strong coupling to the activation process (Olcese et al., 1997), but its gate is associated with the selectivity filter and outer pore entrance of the chan-

nel. The structural basis of coupling between activation and C-type inactivation would be simply explained if the selectivity filter region also participates in activation-related conformational changes. Third, the T442S mutation has been seen in this study not to produce a new class of subconductance states but instead to stabilize existing states that are probably present even in the wild-type channel. A parsimonious explanation for the simultaneous stabilization of all the conducting states would be an allosteric scheme like that in Fig. 11 *B*.

We are grateful to Dr. L.Y. Jan (University of California at San Francisco, San Francisco, CA) for the *Shaker*-NGK2 chimera construct. We also thank Y. Yan for technical assistance with molecular biology and Y. Yang, L. Islas, Q. Jiang, and L. Venkataramanan (all at Yale University) for helpful discussions.

This work was supported by National Institutes of Health grant NS-21501.

Original version received 12 February 1998 and accepted version received 29 July 1998.

REFERENCES

Bezanilla, F., E. Perozo, and E. Stefani. 1994. Gating of *Shaker* K^+ channels: II. The components of gating currents and a model of channel activation. *Biophys. J.* 66:1011–1021.

Chapman, M.L., H.M.A. VanDongen, and A.M.J. VanDongen. 1997. Activation-dependent subconductance levels in the drk1 K channel suggest a subunit basis for ion permeation and gating. *Biophys. J.* 72:708–719.

Cole, K.S., and J.W. Moore. 1960. Potassium ion current in the squid giant axon: dynamic characteristic. *Biophys. J.* 1:1–14.

Colquhoun, D., and F.J. Sigworth. 1995. Fitting and statistical analysis of single-channel records. *In* Single-Channel Recording. 2nd ed. B. Sakmann and E. Neher, editors. Plenum Publishing Corp., New York. 483–588.

Conti, F., I. Inoue, F. Kukita, and W. Stühmer. 1984. Pressure dependence of sodium gating currents in the squid giant axon. *Eur. Biophys. J.* 11:137–147.

De Biasi, M., J.A. Drewe, G.E. Kirsch, and A.M. Brown. 1993*a*. Histidine substitution identifies a surface position and confers Cs^+ selectivity on a K^+ pore. *Biophys. J.* 65:1235–1242.

De Biasi, M., H.A. Hartmann, J.A. Drewe, M. Taglialatela, A.M. Brown, and G.E. Kirsch. 1993*b*. Inactivation determined by a single site in K^+ pores. *Pflügers Arch.* 422:354–363.

Doyle, D.A., J.M. Cabral, R.A. Pfuetzner, A. Kuo, J.M. Gulbis, S.L. Cohen, B.T. Chait, and R. MacKinnon. 1998. The structure of the potassium channel: molecular basis of K^+ conduction and selectivity. *Science.* 280:69–77.

Ferguson, W.B., O.B. McManus, and K.L. Magleby. 1993. Opening and closing transitions for BK channels often occur in two steps via sojourns through a brief lifetime subconductance state. *Biophys. J.* 65:702–714.

Fox, J.A. 1987. Ion channel subconductance states. *J. Membr. Biol.* 97:1–8.

Heginbotham, L., T. Abramson, and R. MacKinnon. 1992. A functional connection between the pores of distantly related ion channels as revealed by mutant K^+ channels. *Science.* 258:1152–1155.

Heginbotham, L., and R. MacKinnon. 1992. The aromatic binding site for tetraethylammonium ion on potassium channels. *Neuron.* 8:483–491.

Hille, B. 1992. Ionic Channels of Excitable Membranes. 2nd ed. Sinauer Associates, Inc., Sunderland, MA. 65–67.

Hoshi, T., W.N. Zagotta, and R.W. Aldrich. 1990. Biophysical and molecular mechanisms of *Shaker* potassium channel inactivation *Science.* 250:533–538.

Hoshi, T., W.N. Zagotta, and R.W. Aldrich. 1991. Two types of inactivation in *Shaker* K^+ channels: effects of alterations in the carboxy-terminal region. *Neuron.* 7:547–556.

Hoshi, T., W.N. Zagotta, and R.W. Aldrich. 1994. *Shaker* potassium channel gating. I: Transitions near the open state. *J. Gen. Physiol.* 103:249–278.

Hurst, R.S., M.P. Kavanaugh, J. Yakel, J.P. Adelman, and R.A. North. 1992. Cooperative interactions among subunits of a voltage-dependent potassium channel. Evidence from expression of concatenated cDNAs. *J. Biol. Chem.* 267:23742–23745.

Hurst, R.S., R. North, and J. Adelman. 1995. Potassium channel assembly from concatenated subunits: effects of proline substitutions in S_4 segments. *Receptors Channels.* 3:263–272.

Isacoff, E.Y., Y.N. Jan, and L.Y. Jan. 1990. Evidence for the formation of heteromultimeric potassium channels in *Xenopus* oocytes. *Nature.* 345:530–534.

Kavanaugh, M.P., R.S. Hurst, J. Yakel, M.D. Varnum, J.P. Adelman, and R.A. North. 1992. Multiple subunits of a voltage-dependent potassium channel contribute to the binding site for tetraethylammonium. *Neuron.* 8:493–497.

Kirsch, G.E., J.A. Drewe, H.A. Hartmann, M. Taglialatela, M. de Biasi, A.M. Brown, and R.H. Joho. 1992. Differences between the deep pores of K^+ channels determined by an interacting pair of nonpolar amino acids. *Neuron.* 8:499–505.

Li, M., N. Unwin, K.A. Stauffer, Y.N. Jan, and L.Y. Jan. 1994. Images of purified *Shaker* potassium channels. *Curr. Biol.* 4:110–115.

Liman, E.R., J. Tytgat, and P. Hess. 1992. Subunit stoichiometry of a mammalian K^+ channel determined by construction of multimeric cDNAs. *Neuron.* 9:861–871.

Liu, D.T., G.R. Tibbs, and S.A. Siegelbaum. 1996*a*. Subunit stoichiometry of cyclic nucleotide-gated channels and effects of subunit order on channel function. *Neuron.* 16:983–990.

Liu, Y., M. Holmgren, M.E. Jurman, and G. Yellen. 1997. Gated access to the pore of a voltage-dependent K^+ channel. *Neuron.* 19: 175–184.

Liu, Y., M.E. Jurman, and G. Yellen. 1996*b*. Dynamic rearrangement of the outer mouth of a K^+ channel during gating. *Neuron.* 16:859–867.

Lopez, G.A., Y.N. Jan, and L.Y. Jan. 1994. Evidence that the S6 segment of the *Shaker* voltage-gated K^+ channel comprises part of the pore. *Nature.* 367:179–182.

Lopez-Barneo, J., and R.W. Aldrich. 1993. Effects of external cations and mutations in the pore region on C-type inactivation of *Shaker* potassium channels. *Receptors Channels.* 1:61–71.

MacKinnon, R. 1991. Determination of the subunit stoichiometry of a voltage-activated potassium channel. *Nature.* 350:232–235.

McCormack, K., L. Lin, L.E. Iverson, M.A. Tanouye, and F.J. Sigworth. 1992. Tandem linkage of *Shaker* K^+ channel subunits does

not ensure the stoichiometry of expressed channels. *Biophys. J.* 63:1406–1411.

Ogielska, E.M., W.N. Zagotta, T. Hoshi, S.H. Heinemann, J. Haab, and R.W. Aldrich. 1995. Cooperative subunit interactions in C-type inactivation of K channels. *Biophys. J.* 69:2449–2457.

Olcese, R., R. Latorre, L. Toro, F. Bezanilla, and E. Stefani. 1997. Correlation between charge movement and ionic current during slow inactivation in *Shaker* K^+ channels. *J. Gen. Physiol.* 110:579–589.

Perozo, E., R. MacKinnon, F. Bezanilla, and E. Stefani. 1993. Gating currents from a nonconducting mutant reveal open-closed conformations in *Shaker* K^+ channels. *Neuron.* 11:353–358.

Schoppa, N.E., K. McCormack, M.A. Tanouye, and F.J. Sigworth. 1992. The size of gating charge in wild-type and mutant *Shaker* potassium channels. *Science.* 255:1712–1715.

Schoppa, N.E., and F.J. Sigworth. 1998*a*. Activation of *Shaker* potassium channels. I. Characterization of voltage-dependent transitions. *J. Gen. Physiol.* 111:271–294.

Schoppa, N.E., and F.J. Sigworth. 1998*b*. Activation of *Shaker* potassium channels. III. An activation gating model for wild-type and V2 mutant channels. *J. Gen. Physiol.* 111:313–342.

Sigworth, F.J. 1994. Voltage gating of ion channels. *Q. Rev. Biophys.* 27:1–40.

Starkus, J.G., L. Kuschel, M.D. Rayner, and S.H. Heinemann. 1997. Ion conduction through C-type inactivated *Shaker* channels. *J. Gen. Physiol.* 110:539–550.

Stühmer, W., F. Conti, M. Stocker, O. Pongs, and S.H. Heinemann. 1991. Gating currents of inactivating and non-inactivating potassium channels expressed in *Xenopus* oocytes. *Pflügers Arch.* 418: 423–429.

Swanson, R., J. Marshall, J.S. Smith, J.B. Williams, M.B. Boyle, K. Folander, C.J. Luneau, J. Antanavage, C. Oliva, S.A. Buhrow, et al. 1990. Cloning and expression of cDNA and genomic clones encoding three delayed rectifier potassium channels in rat brain. *Neuron.* 4:929–939.

Tytgat, J., and P. Hess. 1992. Evidence for cooperative interactions in potassium channel gating. *Nature.* 359:420–423.

Vandenberg, C.A., and F. Bezanilla. 1991. A sodium channel gating model based on single channel, macroscopic ionic, and gating currents in the squid giant axon. *Biophys J.* 60:1511–1533.

Yang, Y., Y. Yan, and F.J. Sigworth. 1997. How does the W434F mutation block current in *Shaker* potassium channels? *J. Gen. Physiol.* 109:779–789.

Yool, A.J., and T.L. Schwarz. 1991. Alteration of ionic selectivity of a K^+ channel by mutation of the H_5 region. *Nature.* 349:700–704.

Zagotta, W.N., T. Hoshi, J. Dittman, and R.W. Aldrich. 1994*a*. *Shaker* potassium channel gating. II: Transitions in the activation pathway. *J. Gen. Physiol.* 103:279–319.

Zagotta, W.N., T. Hoshi, and R.W. Aldrich. 1994*b*. *Shaker* potassium channel gating. III: Evaluation of kinetic models for activation. *J. Gen. Physiol.* 103:321–362.

Zheng, J., and F.J. Sigworth. 1997. Selectivity changes during activation of mutant *Shaker* potassium channels. *J. Gen. Physiol.* 110: 101–117.